Efficient Semi-Blind Channel Estimators for SIMO Systems Suffering From Broadband RFI

Tilahun Melkamu Getu[†‡], Wessam Ajib[‡] and Omar A. Yeste-Ojeda[†]
[†]École de Technologie Supérieure (ÉTS), Montréal, QC, Canada
[‡]Université du Québec À Montréal (UQÀM), Montréal, QC, Canada
tilahun-melkamu.getu.1@ens.etsmtl.ca, ajib.wessam@uqam.ca and Omar.Yeste@lassena.etsmtl.ca

***Abstract*—The effect of broadband radio frequency interference (RFI) is often overlooked in the terrestrial communication literature. However, such an RFI can render very poor equalization for a reception over a frequency selective channel by making the channel estimator perform the worst. Accordingly, the paper firstly proposes an efficient matrix-based semi-blind channel estimator (MB-SCE) for single-input multiple-output (SIMO) systems suffering from severe broadband RFI. Secondly, more-complex yet more performant tensor-based semi-blind channel estimator (TB-SCE) is proposed while showcasing a trade-off between performance and complexity. The paper then compares MB-SCE and TB-SCE with the existing matrix-based blind channel estimator (MB-BCE) and tensor-based blind channel estimator (TB-BCE), respectively, that ignore RFI. Eventually, Matlab® Monte-Carlo simulations have corroborated that MB-SCE and TB-SCE outperform MB-BCE and TB-BCE, respectively. In addition, TB-SCE outperforms MB-SCE especially for a short observation interval.**

I. Introduction

Radio frequency interference (RFI) is prevalent in radio astronomy [1], microwave radiometry [2] and global navigation satellite systems (GNSS) [3]. Furthermore, RFI is also prevalent in systems based on cognitive radio (CR) [4], since spectrum sensing is usually impeded by time and frequency selective mobile radio channel [5].

In addition to CR based systems, terrestrial communications based on OFDM [6]—such as OFDMA in the downlink of LTE/LTE-A [7]—may perform poorly due to a loss of orthogonality rendered by RFI emitted by neighbouring subcarriers which experience severe Doppler spread. Consequently, such an RFI would evoke very poor equalization for a reception over a frequency selective channel by making the channel estimator perform poorly. Nevertheless, proper attention has not been paid to channel estimation in the presence of RFI and the authors come across only contaminated Gaussian log likelihood ratio (CGLLR) based joint iterative channel estimator and decoder [8].

Despite the fact that maximum-likelihood (ML) based estimators are efficient, i.e., achieve the Cramér-Rao lower bound [9], they suffer from a huge computational complexity and the resulting iterative algorithm has no convergence guarantee [10]. On the other hand, subspace-based estimators have lower computational complexity and they often perform close to the Cramér-Rao lower bound [10]. Accordingly, subspace-based estimators are efficient estimators and they have enjoyed tremendous attention in literature.

With the aforementioned motivation in mind, this paper proposes *efficient* semi-blind channel estimators for SIMO systems suffering from severe broaband RFI. To propose efficient estimators, this paper has circumvented the separation of the signal of interest (SOI) subspace from the broadband RFI and noise subspaces by deploying cross-correlation operation between the received signal and pilot (training) symbols. Prior to the cross-correlation operation, the received signal samples from all antennas are arranged to a highly structured vector via a stacking operation. Meanwhile, the SOI subspace has been estimated by employing the singular value decomposition (SVD) of the resulting cross-correlation matrix and the unknown SIMO SOI channel is estimated up to a scalar factor afterwards. Such an efficient channel estimator is named as matrix-based semi-blind channel estimator (MB-SCE).

However, the deployed stacking operation in MB-SCE doesn't reflect the inherent structure of the measurement data and pauses a structural constraint which could evoke a loss of estimation performance. On the otherhand, tensors preserve the inherent structure of the measurement data and structured denoising can be applied which leads to an improved signal subspace estimate enhancing any subspace-based parameter estimation scheme [11]. As a result, this paper proposes tensor-based semi-blind channel estimator (TB-SCE) as an alternative to the proposed MB-SCE while allowing a reasonable complexity. In TB-SCE, truncated higher-order SVD (HOSVD) is applied to the multi-linear equivalent of the abovementioned cross-correlation matrix similar to [12] in order to obtain the tensor-based SOI subspace estimator. Henceforth, the unknown SIMO SOI channel has been estimated up to a scalar factor similar to MB-SCE. Finally, it is worthy noting that the proposed SOI subspace separation scheme can also be used for efficient channel estimation in multiple-input multiple-output (MIMO) systems suffering from broadband RFI. Therefore, a promising foundation for efficient channel estimation in MIMO systems suffering from broadband RFI as well as multi-interferer RFI (MI-RFI) has been laid.

Following this introduction, the paper is organized as follows. Section II presents the notation and system model. Thereafter, MB-SCE is proposed and detailed in Section III. Truncated HOSVD is exploited in Section IV in order to propose TB-SCE which is motivated by the multilinear equivalent of the abovementioned cross-correlation matrix. Section V then presents simulation results followed by paper

978-1-4673-6555-0/15/$31.00 ©2015 IEEE

conclusions which are drawn in Section VI.

II. Notation and System Model

A. Notation

Throughout the paper, scalars, vectors, matrices and tensors are denoted by italic letters, lower-case bold-face letters, upper-case bold-face letters and bold-face calligraphic letters, respectively. The notations $(:,i)$, $||\cdot||_F$, $(\cdot)^T$, $(\cdot)^H$, $\otimes$, $\mathbb{E}\{\cdot\}$ and $\text{vec}(\cdot)$ imply the ith column of a matrix, Frobenius norm, transposition, Hermitian transposition, Kronecker product, expectation operation and vectorization operation, respectively.

The R-dimensional tensor $\boldsymbol{\mathcal{A}} \in \mathbb{C}^{I_1 \times I_2 \times \ldots \times I_R}$ is an R-way array of size I_r along the r-th mode which is consistent with [13]. The r-mode vectors of $\boldsymbol{\mathcal{A}}$ are obtained by varying the r^{th} index, while keeping all other indices fixed and the r-mode unfolding of $\boldsymbol{\mathcal{A}}$ is obtained by collecting all r-mode vectors into a matrix and represented by $[\boldsymbol{\mathcal{A}}]_{(r)} \in \mathbb{C}^{I_r \times I_{r+1} \cdot \ldots \cdot I_R \cdot I_1 \cdot \ldots \cdot I_{r-1}}$. Moreover, the r-rank of $\boldsymbol{\mathcal{A}}$ is defined as the rank of $[\boldsymbol{\mathcal{A}}]_{(r)}$.

The r-mode product of a tensor $\boldsymbol{\mathcal{A}}$ and a matrix $\boldsymbol{U}_r \in \mathbb{C}^{J_r \times I_r}$ is denoted as $\boldsymbol{\mathcal{B}} = \boldsymbol{\mathcal{A}} \times_r \boldsymbol{U}_r$. It is visualized as multiplying the r-mode vectors of $\boldsymbol{\mathcal{A}}$ from left-hand side by the matrix $\boldsymbol{U}_r$, i.e., $[\boldsymbol{\mathcal{B}}]_{(r)} = \boldsymbol{U}_r [\boldsymbol{\mathcal{A}}]_{(r)}$ [14]. For $\boldsymbol{U}_r \in \mathbb{C}^{J_r \times I_r}$ and $\boldsymbol{V}_r \in \mathbb{C}^{K_r \times J_r}$, the r-mode product satisfies [15]

$$(\boldsymbol{\mathcal{A}} \times_r \boldsymbol{U}_r) \times_r \boldsymbol{V}_r = \boldsymbol{\mathcal{A}} \times_r (\boldsymbol{V}_r \,.\, \boldsymbol{U}_r) \tag{1}$$

$$[\boldsymbol{\mathcal{A}} \times_1 \boldsymbol{U}_1 \ldots \times_R \boldsymbol{U}_R]_{(r)} = \boldsymbol{U}_r \,.\, [\boldsymbol{\mathcal{A}}]_{(r)} \,.\, (\boldsymbol{U}_{r+1} \otimes \ldots \otimes \boldsymbol{U}_R \otimes \boldsymbol{U}_1 \otimes \ldots \otimes \boldsymbol{U}_{r-1})^T. \tag{2}$$

B. System Model

We consider a SIMO system with N_R receive antennas suffering from a severe broadband RFI emitted by an interferer equipped with a single antenna. We model the SOI channel between the transmitter and each receive antenna pair as a finite-duration impulse response (FIR) filter with $L+1$ taps [16]. The SOI channel is assumed to be time-invariant for a short-term interval (STI). Similarly, we model the RFI channel between the RFI transmitter and each receive antenna pair as an FIR filter with L_f+1 taps. Like the SOI channel, the RFI channel is also assumed to be time-invariant for an STI. The received signal at time n would then be

$$\boldsymbol{y}(n) = \sum_{l=0}^{L} \boldsymbol{h}_l s(n-l) + \sum_{l=0}^{L_f} \boldsymbol{g}_l f(n-l) + \boldsymbol{z}(n), \tag{3}$$

where $\{\boldsymbol{h}_l, \boldsymbol{g}_l\} \in \mathbb{C}^{N_R}$ are the array response of the N_R antennas corresponding to the lth SOI and RFI, respectively, channel taps, $s(n)$ denotes the symbol emitted by the SOI transmitter at time n, $f(n)$ is the sampled broadband RFI which is usually modeled as a zero mean additive white Gaussian noise (AWGN) [3] and $\boldsymbol{z}(n) \in \mathbb{C}^{N_R}$ is the sampled AWGN with a distribution $\mathcal{N}\big(\boldsymbol{0}, \sigma^2 \boldsymbol{I}_{N_R}\big)$. Furthermore, we assume that the SOI, RFI and noise are uncorrelated and pilot (training) symbols as well as perfect estimates of L and L_f are available.

III. MB-SCE

Like [17], stacking the observation vectors of the N_R receive antennas and W data windows into one highly structured vector of size $N_R.W \times 1$ renders

$$\boldsymbol{y}_n = \boldsymbol{H}\boldsymbol{s}_n + \boldsymbol{G}\boldsymbol{f}_n + \boldsymbol{z}_n, \tag{4}$$

where $\boldsymbol{s}_n = \big[s(nW), \ldots, s(nW - W - L + 1)\big]^T \in \mathbb{C}^{(W+L)}$, $\boldsymbol{f}_n = \big[f(nW), \ldots, f(nW - W - L_f + 1)\big]^T \in \mathbb{C}^{(W+L_f)}$ and $\boldsymbol{z}_n$ denote the sampled data, RFI and zero mean AWGN, respectively. Besides, $\boldsymbol{H} \in \mathbb{C}^{N_R.W \times (W+L)}$ is the SOI filtering matrix defined in [11] and $\boldsymbol{G} \in \mathbb{C}^{N_R.W \times (W+L_f)}$ is the RFI filtering matrix structured as $\boldsymbol{G} = \Big[\boldsymbol{G}_1^T, \boldsymbol{G}_2^T, \ldots, \boldsymbol{G}_{N_R}^T\Big]^T$ for $\boldsymbol{G}_j \in \mathbb{C}^{W \times (W+L_f)}$ being a banded Toeplitz matrix associated with the jth antenna RFI impulse response $\boldsymbol{g}_j \triangleq \Big[g_j^0, \ldots, g_j^{L_f}\Big]^T = \Big[g_j(t_0), \ldots, g_j(t_0 + L_f T_s)\Big]^T$ and

$$\boldsymbol{G}_j = \begin{bmatrix} g_j^0 & \ldots & g_j^{L_f} & 0 & \ldots & \ldots & 0 \\ 0 & g_j^0 & \ldots & g_j^{L_f} & 0 & \ldots & 0 \\ \vdots & \vdots & \vdots & \vdots & \vdots & \vdots & \vdots \\ 0 & \ldots & \ldots & 0 & g_j^0 & \ldots & g_j^{L_f} \end{bmatrix}. \tag{5}$$

Here it shall be noted that t_0 is the time-of-arrival (ToA) and T_s is the symbol duration.

A. SOI Subspace Estimation

Considering the expectation of (4) multiplied by $\boldsymbol{s}_n^H$ while realizing that the SOI, RFI and AWGN are uncorrelated renders

$$\mathbb{E}\{\boldsymbol{y}_n \boldsymbol{s}_n^H\} = \boldsymbol{H}\mathbb{E}\{\boldsymbol{s}_n \boldsymbol{s}_n^H\} + \boldsymbol{G}\mathbb{E}\{\boldsymbol{f}_n\}\mathbb{E}\{\boldsymbol{s}_n^H\} + \mathbb{E}\{\boldsymbol{n}_n\}\mathbb{E}\{\boldsymbol{s}_n^H\}. \tag{6}$$

Recalling that the broadband RFI and AWGN are zero mean Gaussian random variables whilst deploying a sampled cross-correlation confers that

$$\hat{\boldsymbol{R}}_{ys} = \boldsymbol{H}\hat{\boldsymbol{R}}_{ss}, \tag{7}$$

where $\hat{\boldsymbol{R}}_{ys} \approx \frac{1}{N}\sum_{n=1}^{N} \boldsymbol{y}_n \boldsymbol{s}_n^H \in \mathbb{C}^{N_R.W \times (W+L)}$ and $\hat{\boldsymbol{R}}_{ss} \approx \frac{1}{N}\sum_{n=1}^{N} \boldsymbol{s}_n \boldsymbol{s}_n^H \in \mathbb{C}^{(W+L) \times (W+L)}$. In (7), $\hat{\boldsymbol{R}}_{ys}$ and $\boldsymbol{H}$ span identical column space [18]. Consequently, the left singular vectors of $\hat{\boldsymbol{R}}_{ys}$ span the signal subspace $\hat{\boldsymbol{U}}_s$ when we take the economy size SVD of $\hat{\boldsymbol{R}}_{ys}$ for $N_R.W \geq W+L$. Equivalently,

$$\hat{\boldsymbol{R}}_{ys} = \hat{\boldsymbol{U}}_s \hat{\boldsymbol{\Sigma}}_s \hat{\boldsymbol{V}}_s^H, \tag{8}$$

where $\hat{\boldsymbol{U}}_s \in \mathbb{C}^{N_R.W \times (W+L)}$, $\boldsymbol{\Sigma}_s = \text{diag}(\sigma_1, \sigma_2, \ldots, \sigma_r)$ and $r = W + L$. Meanwhile, we assume that $\boldsymbol{S} = [\boldsymbol{s}_1, \boldsymbol{s}_2, \ldots, \boldsymbol{s}_N] \in \mathbb{C}^{(W+L) \times N}$ has a rank of $W + L$, i.e., $N \geq (W + L)$, $\boldsymbol{H}$ has a full column rank, i.e., $N_R.W \geq (W + L)$ and $W > L$ to ensure SOI channel identifiability.

B. SOI Channel Estimation

From (7) and (8), the column space of $\hat{\boldsymbol{U}}_s$ is the linear space spanned by the columns of $\boldsymbol{H}$. Consequently, the unknown SIMO SOI channel coefficients incorporated in the SOI filtering matrix $\boldsymbol{H}$ can be *identified up to a scalar factor* by maximizing the subsequent quadratic form [11] [17]

$$q(\boldsymbol{H}_c) \triangleq \sum_{i=1}^{W+L} \left\| \hat{\boldsymbol{U}}_s(:,i)^H \boldsymbol{H} \right\|_2^2, \tag{9}$$

where $\boldsymbol{H}_c \in \mathbb{C}^{(L+1)\times N_R}$ is a combined SOI channel matrix for all N_R subchannels, i.e., $\boldsymbol{H}_c = \left[\boldsymbol{h}_1, \boldsymbol{h}_2, \ldots, \boldsymbol{h}_{N_R}\right]$. The commutativity $\hat{\boldsymbol{U}}_s(:,i)^T \boldsymbol{H} = \text{vec}(\boldsymbol{H}_c)^T \boldsymbol{D}_i$ [17] assures the dependence of $q(\boldsymbol{H}_c)$ on $\boldsymbol{H}_c$ rather than on $\boldsymbol{H}$, where the matrix $\boldsymbol{D}_i \in \mathbb{C}^{N_R(L+1)\times(L+W)}$ is the filtering matrix associated to the vector $\hat{\boldsymbol{U}}_s(:,i) \in \mathbb{C}^{N_R.W}$ and has the structure $\boldsymbol{D}_i = \left[\boldsymbol{D}_i^{1^T}, \boldsymbol{D}_i^{2^T}, \ldots, \boldsymbol{D}_i^{N_R{}^T}\right]^T$. Each $\boldsymbol{D}_i^j \in \mathbb{C}^{(L+1)\times(L+W)}$ is a banded Toeplitz matrix corresponding to the vector $\hat{\boldsymbol{U}}_s^j(:,i) \in \mathbb{C}^W$, where the vector $\hat{\boldsymbol{U}}_s^j(:,i)$ is obtained by splitting the vector $\hat{\boldsymbol{U}}_s(:,i)$ into N_R sub-vectors, i.e., $\hat{\boldsymbol{U}}_s(:,i) = \left[\hat{\boldsymbol{U}}_s^{1^T}(:,i), \hat{\boldsymbol{U}}_s^{2^T}(:,i), \ldots, \hat{\boldsymbol{U}}_s^{N_R^T}(:,i)\right]^T$.

Hence, the maximization of $q(\boldsymbol{H}_c)$ in (9) boils down to

$$q(\boldsymbol{H}_c) \triangleq \underset{\boldsymbol{H}_c}{\text{argmax}} \quad \text{vec}(\boldsymbol{H}_c)^H . \ \boldsymbol{D} . \ \text{vec}(\boldsymbol{H}_c), \tag{10}$$

where $\boldsymbol{D} = \sum_{i=1}^{W+L} \boldsymbol{D}_i \boldsymbol{D}_i^H$ and the solution of (10) is the eigenvector associated to the largest eigenvalue of $\boldsymbol{D}$ [11] [17].

C. MB-SCE Algorithm

Algorithm I: MB-SCE algorithm

Input: W, L, L_f, N_R, N, $\boldsymbol{Y} = [\boldsymbol{y}_1, \boldsymbol{y}_2, \ldots, \boldsymbol{y}_N]$, $\boldsymbol{S} = [\boldsymbol{s}_1, \boldsymbol{s}_2, \ldots, \boldsymbol{s}_N]$
Assumptions: $N \geq W + L$, $W > L$, $N_R.W \geq W + L$
1: **Initialization**: $i = 1$, $j = 1$, $\boldsymbol{D} = \boldsymbol{0}$
2: $\hat{\boldsymbol{R}}_{ys} = \frac{1}{N} \sum_{n=1}^{N} \boldsymbol{y}_n \boldsymbol{s}_n^H$
3: $\hat{\boldsymbol{R}}_{ys} = \hat{\boldsymbol{U}}_s \hat{\boldsymbol{\Sigma}}_s \hat{\boldsymbol{V}}_s^H$ (economy size SVD); $\hat{\boldsymbol{U}} = \hat{\boldsymbol{U}}_s$
4: **Repeat**
5: $\quad \hat{\boldsymbol{U}}(:,i) = \left[\hat{\boldsymbol{U}}^{1^T}(:,i), \ldots, \hat{\boldsymbol{U}}^{N_R^T}(:,i)\right]^T$
6: $\quad$ **Repeat**
7: $\quad\quad \boldsymbol{D}_i^j \triangleq$ a banded Toeplitz matrix made of $\hat{\boldsymbol{U}}^j(:,i)$
8: $\quad$ **Until** $j = N_R$
9: $\quad \boldsymbol{D}_i = \left[\boldsymbol{D}_i^{1^T}, \ldots, \boldsymbol{D}_i^{N_R^T}\right]^T$, $\boldsymbol{D}_i \in \mathbb{C}^{N_R(L+1)\times(L+W)}$
10: $\quad \boldsymbol{D} = \boldsymbol{D} + \boldsymbol{D}_i \boldsymbol{D}_i^H$
11: **Until** $i = W + L$
12: $\hat{\boldsymbol{H}}_c = \boldsymbol{v}_{\max}$, where $\boldsymbol{D}\boldsymbol{v}_{\max} = \lambda_{\max}\boldsymbol{v}_{\max}$
13: **return** $\xi \hat{\boldsymbol{H}}_c$

In Algorithm I, ξ is the phase ambiguity compensation factor used to compensate the unavoidable *phase ambiguity* evident in blind and/or semi-blind channel estimators whenever the channel is complex [19] and defined as $\xi = a/|a|$ for $a = \text{vec}(\hat{\boldsymbol{H}}_c)^H \text{vec}(\boldsymbol{H}_c)$.

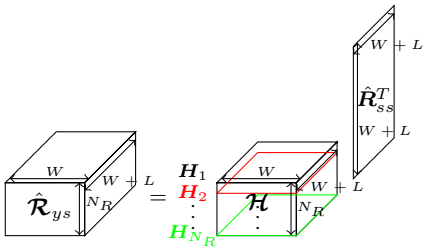

Fig. 1. Multi-linear formulation for $\hat{\boldsymbol{R}}_{ys}$ in (7).

IV. TB-SCE

To deploy the inherent structure of the measurement data, we model the sampled cross-correlation matrix in (7) by a 3-way tensor [11] $\hat{\boldsymbol{\mathcal{R}}}_{ys} \in \mathbb{C}^{N_R\times W\times(W+L)}$. If $\left[\hat{\boldsymbol{\mathcal{R}}}_{ys}\right]_{(3)}^T$ should be equal to $\hat{\boldsymbol{R}}_{ys}$ in (7), the multi-linear equivalent of (7) is

$$\hat{\boldsymbol{\mathcal{R}}}_{ys} = \boldsymbol{\mathcal{H}} \times_3 \hat{\boldsymbol{R}}_{ss}^T, \tag{11}$$

where $\boldsymbol{\mathcal{H}} \in \mathbb{C}^{N_R\times W\times(W+L)}$ is the SOI filtering tensor constructed by aligning the banded Toeplitz matrices $\boldsymbol{H}_j$ of all N_R subchannels along the first dimension as depicted in Fig. 1, i.e., $[\boldsymbol{\mathcal{H}}]_{(3)}^T = \boldsymbol{H}$. Meanwhile, we further assume that $[\boldsymbol{\mathcal{H}}]_{(3)}$ has a full row rank, i.e., $N_R.W \geq (W+L)$ and $W > L$ to ensure SOI channel identifiability.

A. SOI Subspace Estimation

The truncated HOSVD of $\hat{\boldsymbol{\mathcal{R}}}_{ys}$ can be written as [14] [15]

$$\hat{\boldsymbol{\mathcal{R}}}_{ys} \approx \hat{\boldsymbol{\mathcal{S}}}^{[s]} \times_1 \hat{\boldsymbol{U}}_1^{[s]} \times_2 \hat{\boldsymbol{U}}_2^{[s]} \times_3 \hat{\boldsymbol{U}}_3^{[s]}, \tag{12}$$

where $\hat{\boldsymbol{\mathcal{S}}}^{[s]} \in \mathbb{C}^{r_1^s\times r_2^s\times r_3^s}$ is the core tensor which satisfies the all-orthogonality conditions [14], $\hat{\boldsymbol{U}}_1^{[s]} \in \mathbb{C}^{N_R\times r_1^s}$ is a unitary matrix of the singular vectors of $\left[\hat{\boldsymbol{\mathcal{R}}}_{ys}\right]_{(1)}$, $\hat{\boldsymbol{U}}_2^{[s]} \in \mathbb{C}^{W\times r_2^s}$ is a unitary matrix of the singular vectors of $\left[\hat{\boldsymbol{\mathcal{R}}}_{ys}\right]_{(2)}$, $\hat{\boldsymbol{U}}_3^{[s]} \in \mathbb{C}^{(W+L)\times r_3^s}$ is a unitary matrix of the singular vectors of $\left[\hat{\boldsymbol{\mathcal{R}}}_{ys}\right]_{(3)}$ and r_n^s denotes the n-rank of the tensor $\hat{\boldsymbol{\mathcal{R}}}_{ys}$, for $n = 1, 2, 3$. In our SOI subspace estimation, $r_1^s = \min(N_R,\ L+1)$, $r_2^s = \min(W,\ (W+L).\ N_R)$ and $r_3^s = \min(N_R.W,\ W+L)$. Accordingly, $r_2^s = W$ and $r_3^s = W + L$ for the assumption $N_R.W \geq W + L$. The estimated SOI subspace tensor $\hat{\boldsymbol{\mathcal{U}}}^{[s]}$ is then defined as [15]

$$\hat{\boldsymbol{\mathcal{U}}}^{[s]} = \hat{\boldsymbol{\mathcal{S}}}^{[s]} \times_1 \hat{\boldsymbol{U}}_1^{[s]} \times_2 \hat{\boldsymbol{U}}_2^{[s]} \times_3 \hat{\boldsymbol{\Sigma}}_s^{-1}. \tag{13}$$

The columns of $\left[\hat{\boldsymbol{\mathcal{U}}}^{[s]}\right]_{(3)}^T \in \mathbb{C}^{N_R.W\times r_3^s}$ span the estimated SOI subspace and its relationship with $\hat{\boldsymbol{U}}_s$ is stated in the underneath theorem.

Theorem 1: The relationship between tensor-based SOI subspace estimator $\left[\hat{\boldsymbol{\mathcal{U}}}^{[s]}\right]_{(3)}^T$ and matrix-based SOI subspace estimator $\hat{\boldsymbol{U}}_s$ is given by

$$\left[\hat{\boldsymbol{\mathcal{U}}}^{[s]}\right]_{(3)}^T = \left(\hat{\boldsymbol{E}}_1 \otimes \hat{\boldsymbol{E}}_2\right) . \hat{\boldsymbol{U}}_s, \tag{14}$$

where $\hat{\boldsymbol{E}}_r = \hat{\boldsymbol{U}}_r^{[s]} . \hat{\boldsymbol{U}}_r^{[s]^H}$, $r = 1, 2$.

Proof: cf. Appendix A. ∎

Whenever $N_R \leq L+1$, both estimates provide identical result for $\hat{\boldsymbol{E}}_1 \otimes \hat{\boldsymbol{E}}_2 = \boldsymbol{I}_{N_R.W}$. Otherwise, the tensor-based estimate is better that the matrix-based estimate for $\hat{\boldsymbol{E}}_1 \otimes \hat{\boldsymbol{E}}_2 \neq \boldsymbol{I}_{N_R.W}$.

B. SOI Channel Estimation

The SOI channel estimation has also been carried out via (9) and (10) except the replacement of $\hat{\boldsymbol{U}}_s$ by $\left[\hat{\boldsymbol{\mathcal{U}}}^{[s]}\right]_{(3)}^T$.

C. TB-SCE Algorithm

Algorithm II: TB-SCE algorithm

Input: W, L, L_f, N_R, N, $\boldsymbol{Y} = [\boldsymbol{y}_1, \boldsymbol{y}_2, \ldots, \boldsymbol{y}_N]$, $\boldsymbol{S} = [\boldsymbol{s}_1, \boldsymbol{s}_2, \ldots, \boldsymbol{s}_N]$

Assumptions: $N \geq W + L$, $W > L$, $N_R.W \geq W + L$

Initialization: $i = 1$, $j = 1$, $r_1^s = \min(N_R, L+1)$, $r_2^s = \min(W, (W+L).N_R)$, $\boldsymbol{D} = \boldsymbol{0}$

$\hat{\boldsymbol{R}}_{ys} = \frac{1}{N}\sum_{n=1}^{N} \boldsymbol{y}_n \boldsymbol{s}_n^H$ and $\left[\hat{\boldsymbol{\mathcal{R}}}_{ys}\right]_{(3)}^T = \hat{\boldsymbol{R}}_{ys}$

$\hat{\boldsymbol{\mathcal{R}}}_{ys}$ = the tensorization of $\left[\hat{\boldsymbol{\mathcal{R}}}_{ys}\right]_{(3)}$

$[\hat{\boldsymbol{\mathcal{R}}}_{ys}]_{(1)} = \boldsymbol{U}_1 \boldsymbol{\Sigma}_1 \boldsymbol{V}_1^H$; $\hat{\boldsymbol{U}}_1^{[s]} = \boldsymbol{U}_1(:, 1 : r_1^s)$

$[\hat{\boldsymbol{\mathcal{R}}}_{ys}]_{(2)} = \boldsymbol{U}_2 \boldsymbol{\Sigma}_2 \boldsymbol{V}_2^H$; $\hat{\boldsymbol{U}}_2^{[s]} = \boldsymbol{U}_2(:, 1 : r_2^s)$

$\hat{\boldsymbol{R}}_{ys} = \hat{\boldsymbol{U}}_s \hat{\boldsymbol{\Sigma}}_s \hat{\boldsymbol{V}}_s^H$ (economy size SVD)

$\hat{\boldsymbol{U}} = (\hat{\boldsymbol{E}}_1 \otimes \hat{\boldsymbol{E}}_2) . \hat{\boldsymbol{U}}_s$; $\hat{\boldsymbol{E}}_r = \hat{\boldsymbol{U}}_r^{[s]} . \hat{\boldsymbol{U}}_r^{[s]^H}$, $r = 1, 2$

Repeat

  $\hat{\boldsymbol{U}}(:, i) = \left[\hat{\boldsymbol{U}}^{1^T}(:, i), \ldots, \hat{\boldsymbol{U}}^{N_R^T}(:, i)\right]^T$

  Repeat

    $\boldsymbol{D}_i^j \triangleq$ a banded Toeplitz matrix made of $\hat{\boldsymbol{U}}^j(:, i)$

  Until $j = N_R$

  $\boldsymbol{D}_i = \left[\boldsymbol{D}_i^{1^T}, \ldots, \boldsymbol{D}_i^{N_R^T}\right]^T$, $\boldsymbol{D}_i \in \mathbb{C}^{N_R(L+1) \times (L+W)}$

  $\boldsymbol{D} = \boldsymbol{D} + \boldsymbol{D}_i \boldsymbol{D}_i^H$

Until $i = W + L$

$\hat{\boldsymbol{H}}_c = \boldsymbol{v}_{\max}$, where $\boldsymbol{D}\boldsymbol{v}_{\max} = \lambda_{\max}\boldsymbol{v}_{\max}$

return $\xi \hat{\boldsymbol{H}}_c$

V. Simulation Results

For an STI of $N_{\text{tot}}T_s$, we transmitted both Gray-coded 4-QAM pilot symbols and a zero mean AWGN as an RFI over multipath fading channels. To simulate the SOI and RFI multipath fading channels, $(L+1)$- and (L_f+1)-ray multipath continuous-time channels are constructed synchronously using the raised cosine pulse shaping filter $p_{rc}(t, \beta)$ with a roll-off factor of $\beta = 0.5$ and propagation delay $t_0 = 0.1T_s$ as $h_j(t) = \sum_{l=0}^{L} h_j^l p_{rc}(t - lT_s, \beta)$ and $g_j(t) = \sum_{l=0}^{L_f} g_j^l p_{rc}(t - lT_s, \beta)$, for $\{h_j^l, g_j^l\}$ being zero mean i.i.d complex Gaussian random variables with unit variance, respectively [11] [17]. Meanwhile, MB-SCE and TB-SCE are simulated as per Algorithm I and II, respectively, for the succeeding simulation setup.

Both $\boldsymbol{H}$ and $\boldsymbol{G}$ are normalized to a Frobenius norm of $\sqrt{W}$, signal-to-interference-plus-noise ratio (SINR) in [dB] is defined as $\text{SINR} = 10\log_{10}\frac{\mathbb{E}\left\{\left\|\boldsymbol{HS}\right\|_F^2\right\}}{\mathbb{E}\left\{\left\|\boldsymbol{GF}\right\|_F^2\right\}+\mathbb{E}\left\{\left\|\boldsymbol{Z}\right\|_F^2\right\}}$. Similarly, INR in [dB] is defined as $\text{INR} = 10\log_{10}\frac{\mathbb{E}\left\{\left\|\boldsymbol{GF}\right\|_F^2\right\}}{\mathbb{E}\left\{\left\|\boldsymbol{Z}\right\|_F^2\right\}}$, root mean square error (RMSE) is simulated as $\sqrt{\mathbb{E}\left\{\left\|\xi\hat{\boldsymbol{H}}_c - \boldsymbol{H}_c\right\|_F^2\right\}}$ and Tensorlab [20] is deployed for our matricization and tensorization operations. Eventually, Monte-Carlo simulations which average the RMSE over 10,000 channel realizations generate Fig. 2 and Fig. 3.

Fig. 2 compares the performance of the proposed MB-SCE

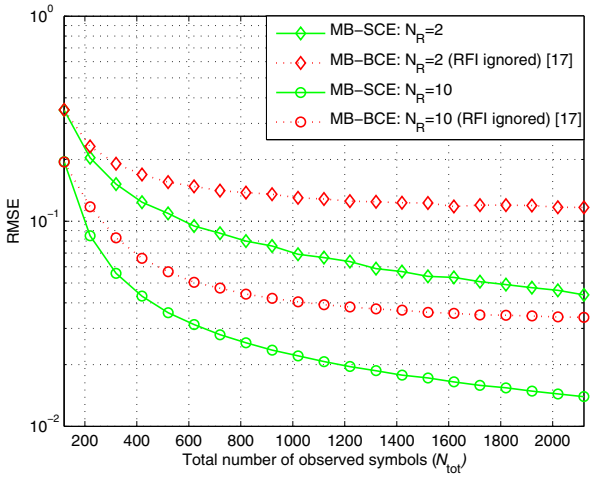

Fig. 2. RMSE performance of MB-SCE and MB-BCE for $W = 10$, $L+1 = L_f + 1 = 3$, SINR = 10 dB, INR = 10 dB and $N_{\text{tot}} = WN$.

with MB-BCE [17] in regard to SIMO systems suffering from broadband RFI. As it is evident from Fig. 2, MB-BCE suffers from a big performance loss as the number of observed symbols for channel estimation increases, since the RFI would be accumulated to disturb the SOI subspace estimation.

Likewise, Fig. 3 compares the performance of TB-SCE

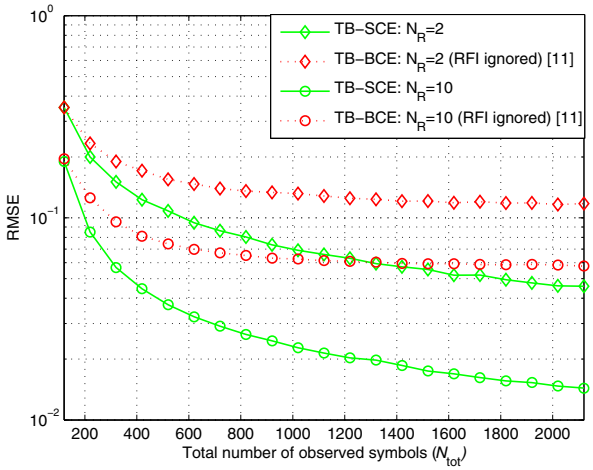

Fig. 3. RMSE performance of TB-SCE and TB-BCE for $W = 10$, $L+1 = L_f + 1 = 3$, SINR = 10 dB, INR = 10 dB and $N_{\text{tot}} = WN$.

with TB-BCE [11] with respect to SIMO systems suffering from broadband RFI. As it is evident from Fig. 3, TB-BCE suffers from a significant performance loss as the number

of observed symbols increases, since the RFI would also be accumulated to disturb the SOI subspace estimation.

Averaging over 100,000 channel realizations produces Fig. 4 which compares MB-SCE and TB-SCE. Whenever $N_R \leq L+1$, MB-SCE and TB-SCE plots overlap. Otherwise, TB-SCE outperforms MB-SCE by virtue of Theorem 1 especially for a short observation interval.

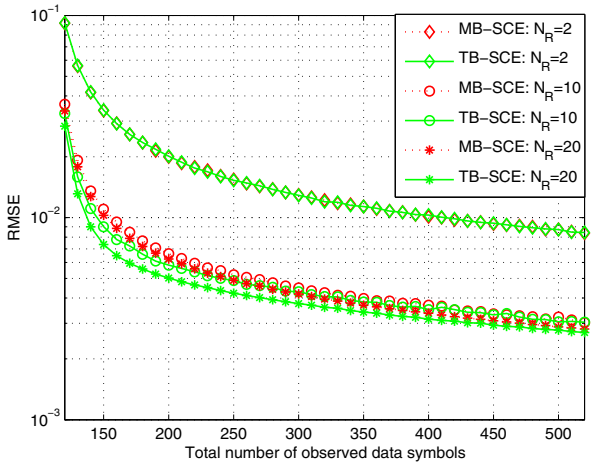

Fig. 4. RMSE performance of MB-SCE and TB-SCE for $W = 10$, $L+1 = L_f + 1 = 3$, SINR $= 30$ dB, INR $= 5$ dB and $N_{\text{tot}} = WN$.

VI. Conclusions

The cross-correlation operation between a received signal and pilot symbols separates the SOI subspace from the broadband RFI as well as noise subspaces. As a result, MB-SCE and TB-SCE are proposed for SIMO systems suffering from severe broadband RFI. Thereafter, the paper compares the proposed semi-blind algorithms with their blind equivalents which ignore RFI after having witnessed RFI being overlooked in literature. Eventually, Monte-Carlo simulations corroborate that MB-SCE and TB-SCE outperform MB-BCE and TB-BCE, respectively. Besides, TB-SCE outperforms MB-SCE. On the other hand, MB-SCE is a low complexity alternative to TB-SCE and performs as good as TB-SCE whenever the number of observed symbols for channel estimation increases.

Appendix A
Proof of Theorem 1

Proof: Having deployed the concept of Theorem 1 and Lemma 1 in [15], the truncated core tensor $\hat{\boldsymbol{\mathcal{S}}}^{[s]}$ is equated as

$$\hat{\boldsymbol{\mathcal{S}}}^{[s]} = \hat{\boldsymbol{\mathcal{R}}}_{ys} \times_1 \hat{\boldsymbol{U}}_1^{[s]^H} \times_2 \hat{\boldsymbol{U}}_2^{[s]^H} \times_3 \hat{\boldsymbol{U}}_3^{[s]^H}. \tag{15}$$

Substituting (15) into (13) and applying (1) afterwards render

$$\hat{\boldsymbol{\mathcal{U}}}^{[s]} = \hat{\boldsymbol{\mathcal{R}}}_{ys} \times_1 \left(\hat{\boldsymbol{U}}_1^{[s]} \,.\, \hat{\boldsymbol{U}}_1^{[s]^H}\right) \times_2 \left(\hat{\boldsymbol{U}}_2^{[s]} \,.\, \hat{\boldsymbol{U}}_2^{[s]^H}\right) \times_3 \left(\hat{\boldsymbol{\Sigma}}_s^{-1} \,.\, \hat{\boldsymbol{U}}_3^{[s]^H}\right). \tag{16}$$

Letting $\hat{\boldsymbol{E}}_r = \hat{\boldsymbol{U}}_r^{[s]} \,.\, \hat{\boldsymbol{U}}_r^{[s]^H}$, for $r = 1, 2$, and taking transposition after applying (2) to (16) result in

$$\left[\hat{\boldsymbol{\mathcal{U}}}^{[s]}\right]_{(3)}^T = \left(\hat{\boldsymbol{E}}_1 \otimes \hat{\boldsymbol{E}}_2\right) \,.\, \left[\hat{\boldsymbol{\mathcal{R}}}_{ys}\right]_{(3)}^T \,.\, \left(\hat{\boldsymbol{U}}_3^{[s]^H}\right)^T \,.\, \hat{\boldsymbol{\Sigma}}_s^{-1}. \tag{17}$$

From (11), $\hat{\boldsymbol{R}}_{ys} = \hat{\boldsymbol{U}}_s \hat{\boldsymbol{\Sigma}}_s \hat{\boldsymbol{V}}_s^H = (\boldsymbol{U}_3 \boldsymbol{\Sigma}_3 \boldsymbol{V}_3^H)^T = \left[\hat{\boldsymbol{\mathcal{R}}}_{ys}\right]_{(3)}^T$. As a result, $\hat{\boldsymbol{V}}_s = \left(\hat{\boldsymbol{U}}_3^{[s]^H}\right)^T$—for r_3^s is always $W + L$—and

$$\left[\hat{\boldsymbol{\mathcal{U}}}^{[s]}\right]_{(3)}^T = \left(\hat{\boldsymbol{E}}_1 \otimes \hat{\boldsymbol{E}}_2\right) \,.\, \hat{\boldsymbol{R}}_{ys} \,.\, \hat{\boldsymbol{V}}_s \,.\, \hat{\boldsymbol{\Sigma}}_s^{-1}. \tag{18}$$

Finally, the direct substitution of (8) into (18) gives

$$\left[\hat{\boldsymbol{\mathcal{U}}}^{[I]}\right]_{(3)}^T = \left(\hat{\boldsymbol{E}}_1 \otimes \hat{\boldsymbol{E}}_2\right) \,.\, \hat{\boldsymbol{U}}_s. \tag{19}$$

■

References

[1] S. van der Tol and A.-J. van der Veen, "Performance analysis of spatial filtering of RF interference in radio astronomy," *IEEE Trans. Signal Process.*, vol. 53, no. 3, pp. 896–910, March 2005.

[2] S. Misra, "Development of radio frequency interference detection algorithms for passive microwave remote sensing," Ph.D. dissertation, Univ. of Michigan, 2011.

[3] M. Wildemeersch and J. Fortuny-Guasch, "Radio frequency interference impact assessment on global navigation satellite systems," EC Joint Research Centre, Security Tech. Assessment Unit, Tech. Rep., Jan. 2010.

[4] S. Haykin, "Cognitive radio: brain-empowered wireless communications," *IEEE J. Sel. Areas Commun.*, vol. 23, no. 2, pp. 201–220, Feb 2005.

[5] J. G. Proakis and M. Salehi, *Digital Communications*, 5th ed. McGraw-Hill, 2008.

[6] H. Schulze and C. Lueders, *Theory and Applications of OFDM and CDMA: Wideband Wireless Communications*. Wiley, 2005.

[7] E. Dahlman, S. Parkvall, and J. Skoeld, *LTE/LTE-Advanced for Mobile Broadband*. Elsevier Ltd., 2011.

[8] P. Insom, R. Liu, R. Duan, Y. Hou, and P. Boonsrimuang, "Joint iterative channel estimation and decoding under pulsed radio frequency interference condition," in *16th Int. Conf. on Advanced Commun. Technology (ICACT)*, Feb 2014, pp. 983–988.

[9] T. A. Schonhoff and A. A. Giordano, *Detection and Estimation Theory and Its Applications*. Prentice-Hall, Inc., 2006.

[10] F. Roemer, "Advanced algebraic concepts for efficient multi-channel signal processing," Ph.D. dissertation, Ilmenau Univ. of Tech., 2012.

[11] B. Song, F. Roemer, and M. Haardt, "Blind estimation of SIMO channels using a tensor-based subspace method," in *proc. the 44th Asilomar Conf. on Signals, Systems and Computers*, Nov 2010, pp. 8–12.

[12] T. M. Getu, W. Ajib, and O. Yeste, "Multi-linear subspace estimation and projection for efficient RFI excision in SIMO systems," in *submission to GlobalSIP'2015*, Orlando, FL, USA, June 2015.

[13] L. D. Lathauwer, B. D. Moor, and J. Vandewalle, "A multilinear singular value decomposition," *SIAM J. Matrix Anal. Appl*, vol. 21, pp. 1253–1278, 2000.

[14] M. Haardt, F. Roemer, and G. Del Galdo, "Higher-order SVD-based subspace estimation to improve the parameter estimation accuracy in multidimensional harmonic retrieval problems," *IEEE Trans. Signal Process.*, vol. 56, no. 7, pp. 3198–3213, July 2008.

[15] F. Roemer, M. Haardt, and G. Del Galdo, "Analytical performance assessment of multi-dimensional matrix- and tensor-based ESPRIT-type algorithms," *IEEE Trans. Signal Process.*, vol. 62, no. 10, pp. 2611–2625, May 2014.

[16] S. Haykin, *Adaptive Filter Theory*, 3rd ed. Prentice-Hall, Inc., 1996.

[17] E. Moulines, P. Duhamel, J. Cardoso, and S. Mayrargue, "Subspace methods for the blind identification of multichannel FIR filters," *IEEE Trans. Signal Process.*, vol. 43, no. 2, pp. 516–525, Feb 1995.

[18] G. Strang, *Introduction to Linear Algebra*, 3rd ed. Wellesley-Cambridge Press, 2003.

[19] L. Tong, G. Xu, and T. Kailath, "A new approach to blind identification and equalization of multipath channels," in *Proc. of Asilomar Conf. on Signals, Systems and Computers*, Nov 1991, pp. 856–860 vol.2.

[20] L. Sorber, M. V. Barel, and L. D. Lathauwer, "Tensorlab v2.0," Jan. 2014. [online]. Available: http://www.tensorlab.net/.